ENCIT 2018

ABCM Associação Brasileira de Engenharia e Ciências Mecânicas

17th Brazilian Congress of Thermal Sciences and Engineering
November 25th-28th, 2018, Águas de Lindóia, SP, Brazil

ENCIT-2018-XXXX
NUMERICAL SIMULATION OF UNSTEADY FLOW IN ENGINE INTAKE AND EXHAUST MANIFOLDS USING THE METHOD OF CHARACTERISTICS

Felipe Augusto Ferreira Gomes
Dr. Waldyr Luiz Ribeiro Gallo
Universidade Estadual de Campinas - UNICAMP
f.augustofgomes@gmail.com
gallo@fem.unicamp.br

Abstract. *The manifolds influence the engine performance and a model capable of estimating the wave action inside them is fundamental. Unsteady three-dimensional models are very expensive and time consuming. However, an one-dimensional approach has shown to be a fair approximation for the problem. There are several numerical methods of different accuracy to conduct an one-dimensional unsteady compressible flow. The method of characteristics (MOC) was one of the first methods to be applied in engine manifolds with reliable results. The method is based on the exact solution and for this reason have good response in the presence of shock waves despite of having first order precision. The volumetric efficiency and the wave behavior were analyzed for different runners length operating between* $1500RPM$ *and* $4000RPM$*. Results showed that volumetric efficiency is heavily influenced by reflected compression waves on intake. However, on exhaust the effect is less significant. For short runners, efficiency demonstrated to have fairly stable variation across engine speed. Nevertheless, up to* 30% *change were detected between low and high speed for longer runners. The* $0.800m$ *intake runner and* $1.000m$ *exhaust presented better performance, with volumetric efficiency above* 90% *for all engine speeds.*

Keywords: *Intake/Exhaust manifolds, One-dimensional flow, Method of Characteristics*

1. INTRODUCTION

The gas exchange processes are responsible for removing the burned gases and to fill the cylinder with a new charge. The intake and exhaust manifolds affect directly volumetric efficiency and residual gas fraction left inside the cylinder after the exhaust process. Since these parameters influence the overall efficiency of the engine, a precise modeling of the unsteady compressible flow inside the manifolds enables a more accurate analysis of the engine performance.

Nowadays, simulations of high resolution can already be done in various ways, which all of them are numerical models. 3D analyses give theoretically the best results, describing the flow field more accurately. However, the complexity of the processes requests a high computational power and time. These models are usually utilized to optimize structural design of the manifolds (Li *et al.*, 2017).

Simpler, cheaper and more suitable solutions to model engine performance can be found. An analysis of compressible one-dimensional flow allows faster simulations of the processes in the manifolds. Although theses simplifications result in loss of information about the flow field, a large number of studies has shown good agreement with empirical data, having average error below 10% (Winterbone and Pearson, 2000; Benson, 1982). An advantage is the low computational time, allowing a simultaneous simulation of the engine. Due to being one-dimensional the models encounter limitations in the presence of valves, junctions, curves and sudden area change inside the pipes, where multidimensional effects become relevant to the flow field. However, correlations and models that take into account those occurrences can be used in conjunction with 1D models (Nikita *et al.*, 2015; Bassett *et al.*, 2003; Winterbone and Pearson, 2000).

Among the one-dimensional models one can find different approaches to estimate the solution of an unsteady compressible flow. One of the first methods applied to internal combustion engines was the method of characteristics (MOC), which is based on the exact solution. Benson *et al.* (1964) developed a finite difference scheme that allowed the implementation of the method. A vast application and validation of the MOC in engines is described in details by Benson (1982). Even though MOC can predict fairly accurately the wave effects, the first order precision of the method hinders wave prediction as the information propagates through time.

Finite volume methods (FVM) have been extensively used to estimate the flow field behavior. A comparison among several FVM methods based on Lax-Wendroff schemes and MOC is presented by (Liu *et al.*, 1996). They showed that the FVM schemes are overall easier to implement and less time-consuming than MOC. However, most of them

presented overshooting of the properties when encountered by shock waves. The exact solution of Gonudov based on the Riemann problem is shown in details by Toro (1999). However, this solution has shown to be very expensive, thus more complex manifolds simulation can become unfeasible very fast. Winterbone and Pearson (2000) describe several high order methods with second order precision in time and space applied to manifold systems. More recently, methods to couple 1D flow with 3D cells have being studied and applied to simulate engine noise (Montenegro *et al.*, 2011).

2. METHODOLOGY

The method of characteristics (MOC) was implemented to simulate the flow inside the manifolds. Although it is a first order accuracy method, MOC is based on the exact solution. Then, it is expected to give an accurate numerical solution when discontinuities in the properties are encountered, such as in shock waves (Smith, 1985). This method consists of reducing first order partial differential equations (PDEs) to ordinary differential equations (ODEs) along specific lines called characteristics.

2.1 Governing equations

The governing equations are the non-conservation laws, taking into account area change, heat transfer and sheer stress on the walls. The equations are; continuity Eq.(1), momentum Eq.(2) and energy Eq.(3).

$$\frac{\partial \rho}{\partial t} + \rho \frac{\partial u}{\partial x} + u \frac{\partial \rho}{\partial x} + \frac{\rho u}{F} \frac{\partial F}{\partial x} = 0 \tag{1}$$

$$\frac{\partial u}{\partial t} + u \frac{\partial u}{\partial x} + \frac{1}{\rho} \frac{\partial p}{\partial x} + \frac{4f}{D_h} \frac{u^2}{2} \frac{u}{|u|} = 0 \tag{2}$$

$$\frac{\partial p}{\partial t} + u \frac{\partial p}{\partial x} - a^2 \left(\frac{\partial \rho}{\partial t} + u \frac{\partial \rho}{\partial x} \right) - (k-1)\, \rho \left(q + u \frac{4f}{D_h} \frac{u^2}{2} \frac{u}{|u|} \right) = 0 \tag{3}$$

where F is the area, q is the heat transfer rate through walls, f is the wall friction factor, ρ is density, u is flow velocity, p is pressure, a is the speed of sound and D_h is the hydraulic diameter. Equation (1) to (3) can be interpreted as a set of non-linear hyperbolic partial differential equations. These expressions accept solution along specific lines in the space-time plane called characteristic curves. Equation (4) represents the lines in which the solution is valid.

$$\frac{dx}{dt} = u \pm a \qquad \text{and} \qquad \frac{dx}{dt} = u \tag{4}$$

Along these line the total differential of the properties is valid, thus the system of equations can be reduced to Eq.(5) and Eq.(6). Benson (1982) and Winterbone and Pearson (2000) give a detailed explanation on how to obtain this solution.

$$\frac{dp}{dt} \pm \rho a \frac{du}{dt} - (k-1)\rho \left(q + u \frac{4f}{D_h} \frac{u^2}{2} \frac{u}{|u|} \right) + \frac{\rho u a^2}{F} \frac{dF}{dx} \pm \rho a \frac{4f}{D_h} \frac{u^2}{2} \frac{u}{|u|} = 0 \tag{5}$$

$$\frac{dp}{dt} - a^2 \frac{d\rho}{dt} - (k-1)\rho \left(q + u \frac{4f}{D_h} \frac{u^2}{2} \frac{u}{|u|} \right) = 0 \tag{6}$$

Benson (1982) introduces a variable named entropy level, a_A, which represents the sound speed of the fluid if it suffered a isentropic expansion until the reference pressure, Eq.(7).

$$\frac{a}{a_A} = \left(\frac{P}{P_{ref}} \right)^{(k-1)/(2k)} \tag{7}$$

It is convenient to write all equations in a non-dimensional form, where the properties are expressed by Eq.(8). The set of equations can then be expressed by Eq.(9) and Eq.(10).

$$A = \frac{a}{a_{ref}}, \qquad U = \frac{u}{a_{ref}}, \qquad Z = t \frac{a_{ref}}{L_{ref}}, \qquad X = \frac{x}{L_{ref}}, \qquad A_A = \frac{a_A}{a_{ref}} \tag{8}$$

$$\frac{(dA \pm \frac{k-1}{2}dU)}{dZ} = \frac{k-1}{2}\frac{AU}{F}\frac{dF}{dX} + \frac{A}{A_A}dA_A \\ \mp \frac{k-1}{2}\frac{2fL_{ref}}{D}U^2\frac{U}{|U|}\left(1-(k-1)\frac{U}{A}\right) + \frac{(k-1)^2}{2}\frac{qL_{ref}}{a_{ref}}\frac{1}{A} \tag{9}$$

$$\frac{dA_A}{dZ} = \frac{k-1}{2}\frac{A_A}{A^2}\left(\frac{qL_{ref}}{a_{ref}^3} + \frac{2fL_{ref}}{D}|U^3|\right) \tag{10}$$

It is possible to decouple Eq.(9), facilitating the solution, by making a variable substitution Eq.(11). Integrating such equation, it is defined two new properties called Riemann variables, Eq.(12).

$$d\lambda = dA + \left(\frac{k-1}{2}\right)dU \qquad \text{and} \qquad d\beta = dA - \left(\frac{k-1}{2}\right)dU \tag{11}$$

$$\lambda = A + \frac{k-1}{2}U \qquad \text{and} \qquad \beta = A - \frac{k-1}{2}U \tag{12}$$

λ represents the propagation of the wave from the left to the right of a pipe and β on the opposite direction. All the properties and the slope of the characteristics can be written as a function of λ, β and A_A, Eq(13) and Eq.(14), respectively.

$$A = \frac{\lambda+\beta}{2}, \qquad U = \frac{\lambda-\beta}{k-1}, \qquad P = P_{ref}\left(\frac{\lambda+\beta}{2A_A}\right)^{2k/(k-1)} \tag{13}$$

and

$$\left(\frac{dX}{dZ}\right)_\lambda = b\lambda - a\beta, \qquad \left(\frac{dX}{dZ}\right)_\beta = a\lambda - b\beta, \qquad \left(\frac{dX}{dZ}\right)_{A_A} = \frac{\lambda-\beta}{k-1} \tag{14}$$

where $a = (3-k)/(2k-2)$ and $b = (k+1)/(2k-2)$. Substituting the properties as functions of Riemann variables on Eq.(9) and Eq.(10) creates a new set of equations depending only on λ, β and A_A. Those equations can be solved numerically by a mesh method.

In laminar flow regime, Reynolds number below 2000, the friction factor is given by $f = 64/Re$. For turbulent flow the Colebrook equation, Eq.(15), was considered and solved by iterative manner, where Re is the Reynolds number and ϵ the pipe's roughness. The heat transfer was calculated by Reynold's analogy, Eq.(16) (Winterbone and Pearson, 2000).

$$\frac{1}{\sqrt{f}} = -2.0\log\left(\frac{\epsilon/D}{3.7} + \frac{2.51}{Re\sqrt{f}}\right) \tag{15}$$

$$q = \frac{2f}{D}\frac{k}{k-1}R|u|\left(T_{wall} - T_{gas}\right) \tag{16}$$

2.2 Numerical procedure

The mesh is assumed rectangular with ΔX constant and predefined. Since the Courant stability criterion must be satisfied for every mesh point, a single time step ΔZ is adjusted in every new iteration using Eq.(17) in a manner that this criterion is always fulfilled for the whole mesh.

$$\Delta Z \leq \frac{\Delta X}{(A+|U|)_{max}} \tag{17}$$

Figure 1 illustrates the logic with both characteristics arriving at i at time $n+1$ for subsonic flow and $u > 0$. For small time steps, λ and β curves can be assumed as straight lines. The Courant stability criterion guarantees that L, R and K are always between $i-1$ and $i+1$. The properties values at those points are interpolated between the adjacent

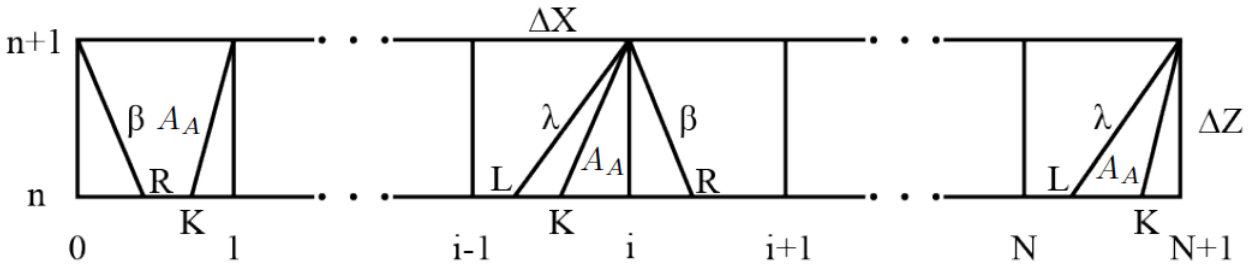

Figure 1. Mesh Grid

nodes. Equation (18) demonstrates a interpolation for a point on the left of i, if it was to be on the right ϕ_{i+1} should be used instead of ϕ_{i-1}.

$$\phi_P = \phi_i - \left(\frac{\delta X}{\Delta X}\right)_P (\phi_i - \phi_{i-1}) \tag{18}$$

Where ϕ represents any property, P one of the points L, R or K, δx is the distance between the mesh point i and the point to be interpolated. $\delta X/\Delta X$ can be determined by the slope dX/dZ, resulting in Eq.(19) to (21)

$$\left(\frac{\delta X}{\Delta X}\right)_\lambda = \frac{b\lambda_i - a\beta_i}{\frac{\Delta X}{\Delta Z} + b\left(\lambda_i - \lambda_{i-1}\right) - a\left(\beta_i - \beta_{i-1}\right)} \tag{19}$$

$$\left(\frac{\delta X}{\Delta X}\right)_\beta = \frac{a\lambda_i - b\beta_i}{\frac{\Delta X}{\Delta Z} + a\left(\lambda_i - \lambda_{i+1}\right) - b\left(\beta_i - \beta_{i+1}\right)} \tag{20}$$

$$\left(\frac{\delta X}{\Delta X}\right)_{A_A} = \frac{\lambda_i - \beta_i}{\frac{\Delta X}{\Delta Z}(k-1) + \left(\lambda_i - \lambda_{i-1}\right) - \left(\beta_i - \beta_{i-1}\right)} \tag{21}$$

The solution can be obtained in the form of Eq.(22), where the derivatives are given by Eq.(9) and Eq.(10). The entropy level equation must be solved first since Eq.(9) needs the value of $A_{A_i}^{n+1}$ in order to be resolved.

$$\lambda_i^{n+1} = \lambda_L^n + \left(\frac{d\lambda_L}{dZ}\right) dZ, \qquad \beta_i^{n+1} = \beta_R^n + \left(\frac{d\beta_R}{dZ}\right) dZ, \qquad A_{A_i}^{n+1} = A_{A_k}^n + \left(\frac{dA_{A_K}}{dZ}\right) dZ \tag{22}$$

The described procedure for calculating the new Riemann variables and the entropy level at the nodes, and consequently the properties at each node, was done from $i = 1$ to $i = N + 1$ for λ and from $i = 0$ to $i = N$ for β. The entropy level is estimated at the boundaries when possible, if not the value from previous iteration is considered. The boundary conditions estimate the correct values of $\lambda_{i=0}$, $\beta_{i=N+1}$ and A_A when needed.

2.3 Boundary conditions

Benson (1982) and Winterbone and Pearson (2000) describe how to conduct a proper analysis of the boundaries using MOC. The flow is assumed to be quasi-steady when applied to an infinitesimal small region. This suggests that the size of the boundary is too small compared to the size of the pipe and that $d/dx \gg d/dt$. Since the process is considered quasi-steady, flow direction is defined by difference in pressure.

At the boundaries the Riemann variables are redefined as λ_{in} for the waves approaching a boundary and λ_{out} for the ones leaving it. This way, λ_{out} represents the estimated solution for λ or β at time $n + 1$, depending on which pipe end is the boundary. The entropy level and λ_{in} must be corrected in case of inflow since the gas mixture of different temperatures changes entropy. This correction is done by including Eq.(23) to the set of equations. λ_{in_n} and A_{A_n} are the arriving characteristics calculated by the normal procedure. Notice that Eq.(23) is implicit and therefore needs iterative solution.

$$\lambda_{in} = \lambda_{in_n} + \left(\frac{\lambda_{in} + \lambda_{out}}{2}\right)\left(\frac{A_A - A_{A_n}}{A_A}\right) \tag{23}$$

The used boundaries in this work were only valve and open end. However, flow going into and out of the pipe must be treated differently.

2.3.1 Valve - flow going into the pipe

The expressions are derived from the continuity and energy equations between the cylinder, throat and pipe. It is assumed that the gas leaves a cylinder with stagnation pressure P_c and expands isotropically. After, in the throat, it expands but changing its entropy level. From continuity and energy equations, it can be shown that Eq.(24), to (27) represents the solution for flow going into the pipe, where Eq.(26) must be used for subsonic flow and Eq.(27) for chocked flow instead. The subscript 'c' represents the cylinder. Equation (23) completes the set of equations which is solved numerically by Benson (1982)'s approach.

$$\lambda_{out} = \frac{a\lambda_{in} + \sqrt{2bA_c^2 + \lambda_{in}\left(a^2 - b^2\right)}}{b} \tag{24}$$

$$A_A = \left(\frac{\lambda_{out} + \lambda_{in}}{2}\right)\left(\frac{P_c}{P} \cdot \frac{P_{ref}}{P_c}\right)^{(k-1)/2k} \tag{25}$$

$$\frac{P}{P_c} = \left[\frac{1}{2C}\left(\psi\sqrt{\psi^2 + 4C} - \psi^2\right)\right]^{k/(k-1)}, \qquad \text{where} \qquad C = \frac{\left(\frac{k-1}{2}\right)\left(\frac{\lambda_{out} - \lambda_{in}}{k-1}\right)^2}{\left[1 - \left(\frac{k-1}{2}\right)\left(\frac{\lambda_{out} - \lambda_{in}}{k-1}\right)^2\right]^2} \tag{26}$$

$$\frac{P}{P_c} = \psi\left(\frac{2}{k+1}\right)^{(k+1)/2(k-1)}\left[1 - \frac{k-1}{2}\left(\frac{\lambda_{out} - \lambda_{in}}{k-1}\right)^2\right]\left(\frac{k-1}{\lambda_{out} - \lambda_{in}}\right) \tag{27}$$

2.3.2 Valve - flow going out the pipe

Similar analysis is made for flow leaving the pipe. From continuity and energy equations, the solution for subsonic flow corresponds to Eq.(28), where A is calculated numerically from Eq.(29) and Eq.(30).

$$\lambda_{out} = (2A - \lambda_{in}) \tag{28}$$

$$\left[(A^*)^{4/(k-1)} - \psi^2\right](\lambda_{in}^* - A^*) - \frac{k-1}{2}\psi^2\left(A^{*^2} - 1\right) = 0 \tag{29}$$

$$A^* = \frac{A}{A_A\left(\frac{P_b}{P_{ref}}\right)^{(k-1)/2k}}, \qquad \lambda_{in}^* = \frac{\lambda_{in}}{A_A\left(\frac{P_b}{P_{ref}}\right)^{(k-1)/2k}} \tag{30}$$

If chocked flow is encountered, the solution may be written as Eq.(31) and Eq.(32), where A_{cr}^* is estimated by numerically solving Eq.(33).

$$\lambda_{out} = K_s\lambda_{in} \tag{31}$$

$$K_s = \frac{1 - \frac{k-1}{2}\psi\left(\frac{1}{A_{cr}^*}\right)^{(k+1)/(k-1)}}{1 + \frac{k-1}{2}\psi\left(\frac{1}{A_{cr}^*}\right)^{(k+1)/(k-1)}} \tag{32}$$

$$\psi^2 - \left(\frac{k+1}{k-1} - \frac{2}{k-1}A_{cr}^{*^2}\right)(A_{cr}^*)^{4/(k-1)} = 0 \tag{33}$$

2.3.3 Valve - closed

When the valve is closed the incident wave is completely reflected and flow velocity must be zero. This corresponds to $\lambda_{out} = \lambda_{in}$.

2.3.4 Open End - flow going out the pipe

The solution for a flow going out to an environment of pressure P_b is expressed in Eq.(34). This equation is derived from the fact that the pressure in the pipe must be the same as the outside pressure, $P = P_b$.

$$\lambda_{out} = 2A_A \left(\frac{P_b}{P_{ref}} \right)^{(k-1)/2k} - \lambda_{in} \tag{34}$$

2.3.5 Open End - flow going into the pipe

Since inflow, λ_{in} must be corrected by Eq.(23). From energy equation it can be shown that the reflected characteristic is given by Eq.(35) for subsonic flow and Eq.(36) in case of chocked flow.

$$\lambda_{out} = \frac{a\lambda_{in} + \sqrt{2bA_c^2 + \lambda_{in}\left(a^2 - b^2\right)}}{b} \tag{35}$$

$$\lambda_{out} = \lambda_{in} \left(\frac{k+1}{3-k} \right) \tag{36}$$

2.4 Simulations

Figure 3 shows the simulated scheme. It was considered non-homeotropic flow in the pipes. Where, in one end there is a valve and in the opposite end is opened to atmosphere. The diameter of the runners are $0.508m$ and the ports are $0.0300m$. It was considered that the length of the ports are too small compared to the length of the runners. Therefore, the ports only affect the curtain area of the valves. The properties of the gases inside the runners were considered constant.

The simulations were conducted varying one of the runners length from $0.300m$ to $1.300m$ in $0.020m$ steps and engine speeds from $1500RPM$ to $4000RPM$ in $500RPM$ steps, while the other runner stayed fixed at $0.600m$. The discretization length for both runners was $0.010m$.

The simulated engine follows the description displayed in the Tab.1 and the valves lift profiles in Fig.2. The simulation ran with gasoline as fuel working at stoichiometric relation. The combustion model is based on a single Wiebe function. The volumetric efficiency is defined as the actual mass of mixture consumed by the engine divided by the ideal mass of mixture that could be drawn in based on displacement volume Eq.(37).

$$\eta_V = \frac{m_{real}}{\frac{P_{atm}V_{disp}}{RT_{atm}}} \tag{37}$$

Table 1. Engine characteristics

Engine type	4 stroke
Bore and Stroke	80.0 x 80.0mm
Displacement	400cc
Valve Timing	
i.v.o	700°
i.v.c	210°
e.v.o	490°
e.v.c	15°
Compression Ratio	12.5
Intake Valve Diam	30.93mm
Exhaust Valve Diam	28.27mm

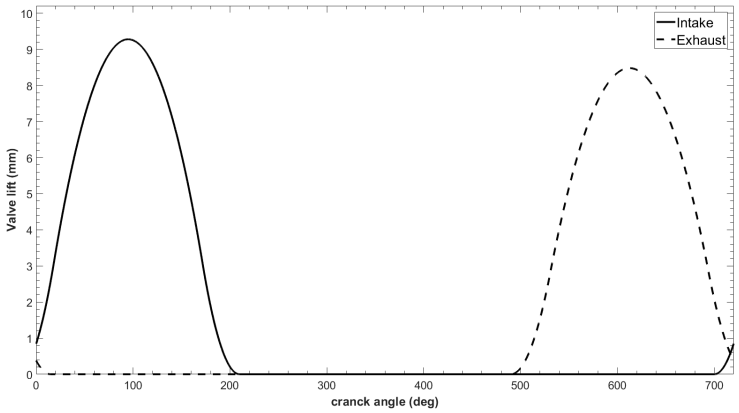

Figure 2. Valves lift profile

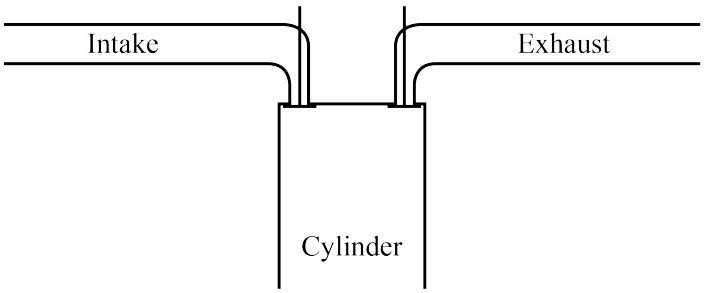

Figure 3. Manifold-Cylinder system used in the simulations

3. RESULTS

3.1 Describing the phenomenon

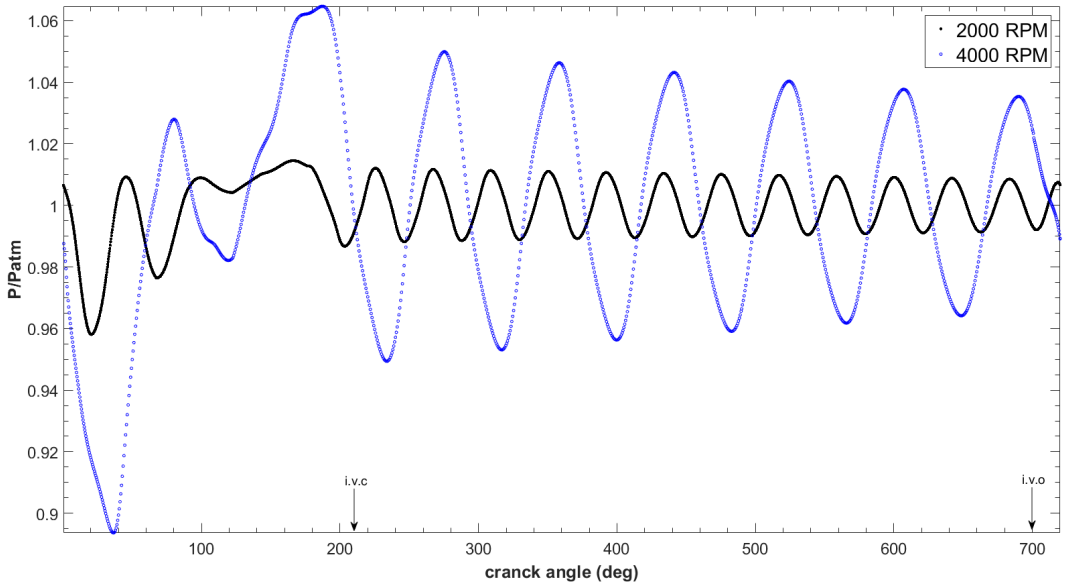

Figure 4. Intake pressure at valve end in $0.300m$ runner

For the system in Fig.3, two types of wave are encountered: compression wave and rarefaction wave. In the intake manifold, a rarefaction wave appears at the inlet valve when the cylinder pressure drops as the piston moves downward.

This wave propagates to the open end of the pipe and is reflected back to the valve as a compression wave (Heywood, 1989). The arrival of this wave, while the valve is still open, allows an increase in mass flow. Adjusting the length to maximize this phenomena is called tunning and is vastly used in runner design. If timed correctly the compression wave may work as a compressor, "pushing" additional air capable of increasing volumetric efficiency above 100%. When the valve is closed, the waves are reflected without any change. Thus, during the closed phase the waves travel back and forth purely reflecting at the closed valve and inverting at the open end. For the exhaust runner similar behavior is faced, after the valve is opened a compression wave propagates outward and is inverted as a rarefaction wave traveling back to the valve. The arrival of such wave helps the cylinder clearance and consequently increases volumetric efficiency.

Figures 4 and 5 describe the pressure, normalized by atmospheric pressure, at the inlet valve at $2000RPM$ and $4000RPM$ for a runner of $0.300m$ and $1.000m$, respectively. The shorter runner has volumetric efficiency of 93.8% and 91.7% at $2000RPM$ and $4000RPM$, respectively, while the longer has 100.6% and 88.1%. On one hand, it can be seen that the shorter runner presents more reflected waves than the longer pipe and its pressure peaks are much lower. This is due to the wave having more time to expand in the longer runner, increasing its intensity. On the other hand, rising speed reduces the reflection frequency due to less time for the waves to propagate. It also significantly increases the pressure peaks.

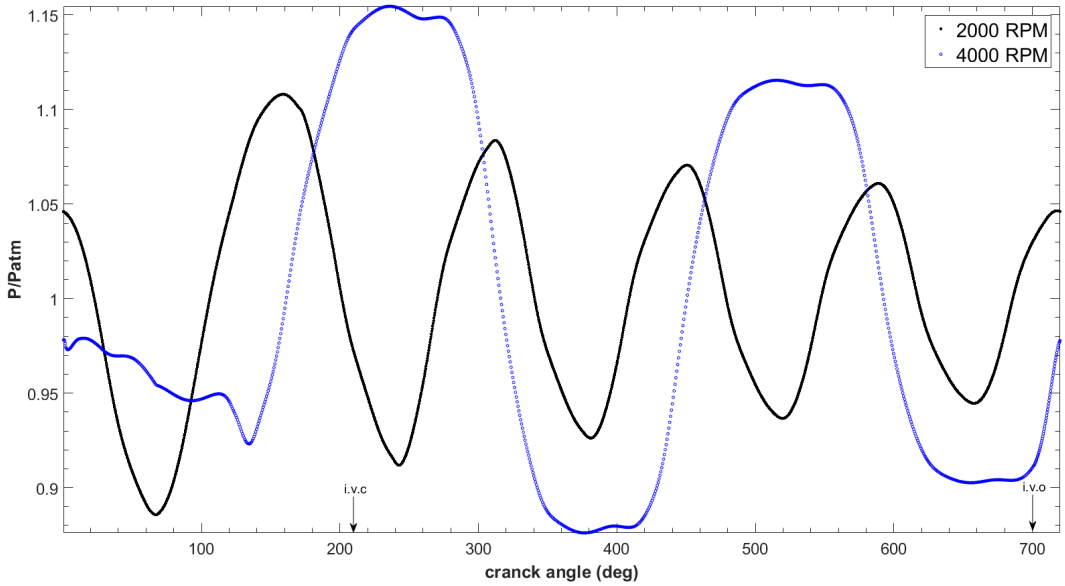

Figure 5. Intake pressure at valve end in $1.000m$ runner

During the opened valve period, there was time for the arrival of four pressure waves in the $0.300m$ runner at $2000RPM$ and three at $4000RPM$ while the longer runner showed only two at $2000RPM$ and barely one at $4000RPM$. The pressure peaks for the $1.000m$ are overall about 10% greater compared to the shorter runner at the same speeds. The first pressure peak occurs in the early stages of the open valve, then not having a huge influence in the mass flow. In both runners, the compression waves diminish in strength with each reflection due to friction losses. As expected, the longer runner has greater pressure peak drop. In addition, the increase in speed also results in a higher pressure peak drop. This is caused by the increase in flow friction associated with the high flow speed at the runners at $4000RPM$.

The determinant factor for the volumetric efficiency is the mass flow, which is heavily influenced by pressure ratio between the cylinder and the port. A higher number of the compression waves arriving at the opened valve does not necessarily mean greater efficiency. After a "charge" due to a compression wave, the cylinder pressure also increases, hindering the mass flow afterwards. This can be observed comparing the shorter runner with the longer one both at $2000RPM$. Although there are more compression waves arriving at the valve in the $0.300m$ runner at $2000RPM$, it presented lower volumetric efficiency. For the $1.000m$, there is only one high pressure wave arriving during the valve open phase. Therefore, promoting a higher mass flow inwards the cylinder reflected in a greater volumetric efficiency. On the other hand, the longer runner at $4000RPM$ showed the lowest volumetric efficiency. This fact is attributed to the compression wave arriving when the valve is almost closed, then not contributing to increase mass flow.

In the exhaust system, Fig.(6), the wave behavior is analogous regarding wave propagation and reflection. However, rarefaction waves arrive at the valve instead of compression waves. The high flow speed promotes more reflections and higher flow friction compared to intake's. Rising engine speed and extending runner length also reduced the number of reflections for the same reasons explained before. A higher pressure difference provokes better clearance, which improves

volumetric efficiency.

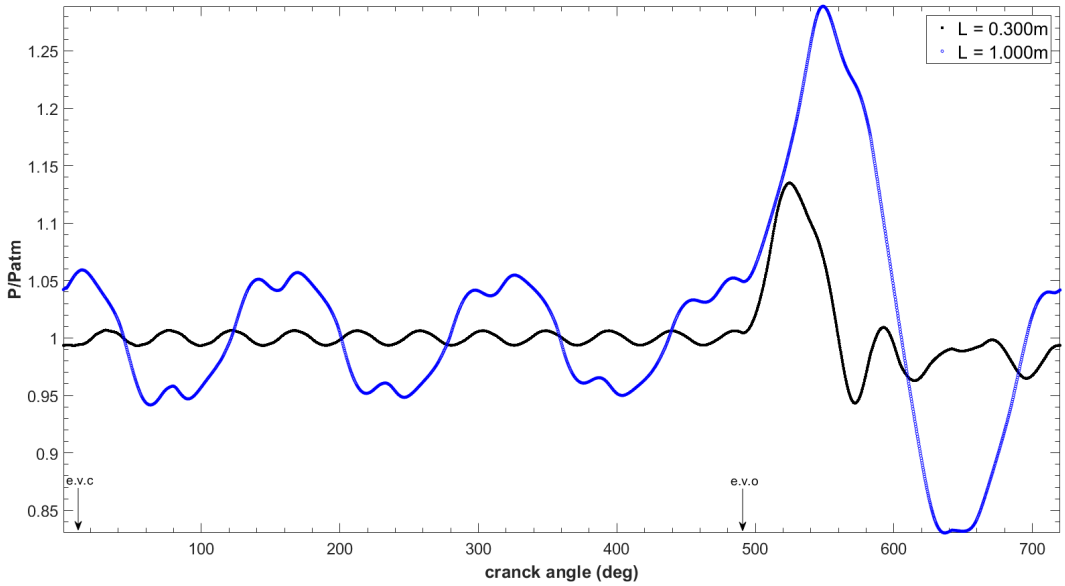

Figure 6. Exhaust pressure at valve end at $4000RPM$

3.2 Variable Runners

Figure 7 illustrates the volumetric efficiency for intake runners varying from 0.300 to 1.300 meters and engine speed varying from 1500 to $4000RPM$. The highest observed efficiency was 106.2% for runner of $1.260m$ at $2000RPM$ and the lowest was 74.6% for $1.300m$ at $4000RPM$. Engine speeds from $2000RPM$ to $3000RPM$ showed efficiency above 100% at some point, meaning that the arriving of a compression wave worked as a compressor. Every runner with length below $0.800m$ demonstrated volumetric efficiency above 90% for all engine speeds.

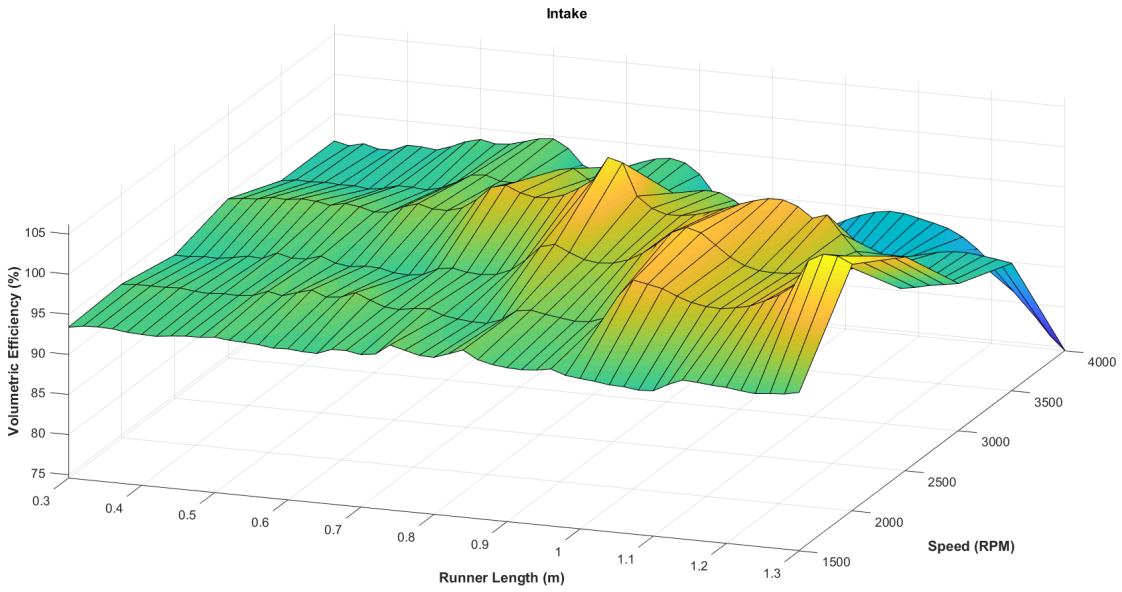

Figure 7. Volumetric efficiency for variable intake runner

Between $0.300m$ and $0.600m$, the efficiency had small variation, around only 2.5% for each speed, with $3500RPM$ being the one with the highest change, 91.7% to 94.9%. Overall the efficiency varied between around 91% and 96% among all speeds. Subsequent $0.6m$ sharper changes were shown by $3000RPM$ and above. The lower speeds encountered more

significant changes with longer runners, except for $1500RPM$ that remained fairly stable for all lengths. As described before, this is due to the compression waves having small intensity at low speeds. However, longer runners have greater pressure peaks and consequently having bigger impact on volumetric efficiency. In addition, these runners showed a wider range, in which the $1.300m$ runner showed a difference in efficiency over 30% across $1500RPM$ and $4000RPM$. All of the smallest efficiencies were perceived at $4000RPM$, being the only speed to present efficiency below 85%. Its efficiency rapidly drops after $0.800m$ runner due to no compression wave arriving during the valve open phase, as illustrated in Fig 5 for $4000RPM$. The $0.800m$ runner showed to have the best overall performance, with all speeds having volumetric efficiency above 90% and even above 100% for $3000RPM$.

Figure 8 provides the volumetric efficiency for exhaust runners. The greatest peak was detected for $1.240m$ runner at $2000RPM$, 97.0%, while the smallest efficiency happened for $1.300m$ at $1500RPM$. The exhaust runner length showed a much lower influence on the volumetric efficiency than the intake's. This is due to the high compression ratio of the engine. When the exhaust valve opens, the cylinder pressure is high enough to already guarantee a good clearance. Therefore, the rarefaction waves arriving at the open valve do not have a huge contribution. In general, changing runners length caused smooth variations on volumetric efficiency. However, every speed, except $3000RPM$ and $3500RPM$, showed a sudden increase between $0.840m$ and $1.220m$. Opposite to intake, the slowest speed presented the largest change, from 89.2% to 95.9%, and all of the smallest values in volumetric efficiency. However, regarding engine speed the behavior was very similar to intake's. Runners until $0.800m$ demonstrated uniform changes across different speeds, while the longer pipes showed larger volumetric efficiency variation. The $1.300m$ runner had the widest range, from 89.2% to 96.6%. Overall, the best performing runner was $1.000m$, with volumetric efficiency above 92% for all speeds and encountering two efficiency peaks, for $1500RPM$ and $2500RPM$.

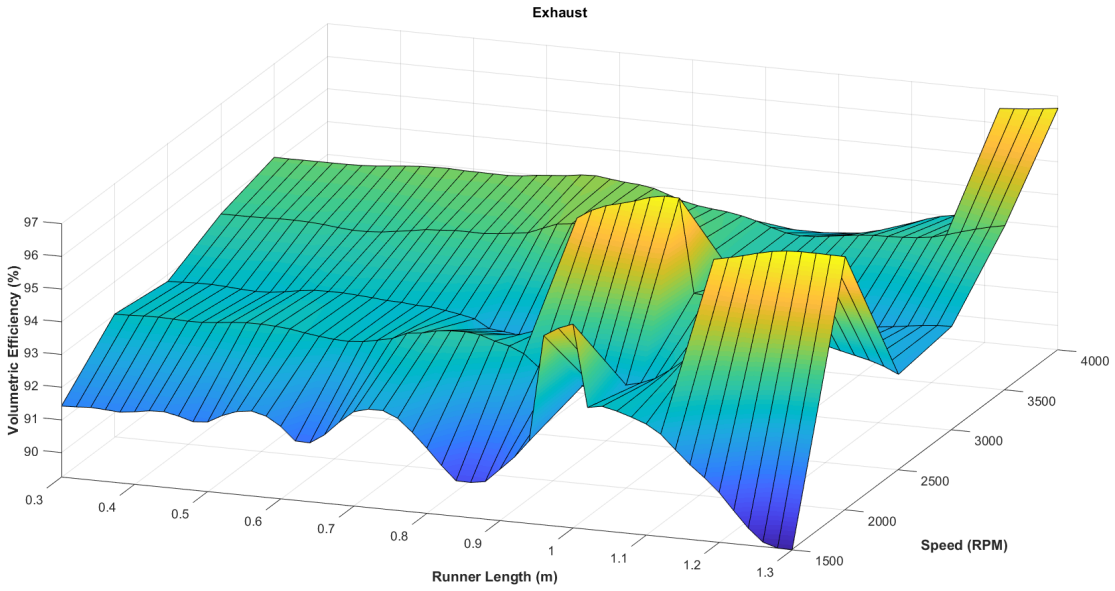

Figure 8. Volumetric efficiency for variable exhaust runner

4. CONCLUSIONS

The extension of runner's length resulted in a growth of intensity pressure peak and reduction on reflected wave despite of increasing flow friction. Moreover, higher speeds showed the same trends. This behavior appeared for intake and exhaust runners. Volumetric efficiency was way affected by intake runner length than exhaust, varying over 20% for high engine speeds. For both systems, the volumetric efficiency for shorter runners presented more uniform variation along the speed range. However, longer runners showed significant differences between low and high speeds, up to 30% for intake's. At $1500RPM$ the change on intake runner length has the least impact on volumetric efficiency of all speeds, around 2%. Nevertheless, varying the exhaust runner showed the opposite behavior having the highest change among all speeds, around 6%. The overall better performing runners were $0.8m$ for intake and $1.0m$ for exhaust. Both runners presented volumetric efficiency above 90% for every speed and even above 100% for $3000RPM$.

5. ACKNOWLEDGEMENTS

We would like to thank CAPES for helping this project by funding through a master's scholarship.

6. REFERENCES

Bassett, M.D., Pearson, R.J., Fleming, N.P. and Winterbone, D.E., 2003. "A Multi-Pipe Junction Model for One-Dimensional Gas-Dynamic Simulations". doi:10.4271/2003-01-0370. URL http://papers.sae.org/2003-01-0370/.

Benson, R.S., 1982. *The Thermodynamics and Gas Dynamics of Internal Combustion Engines Volume 1*. Oxford : Clarendon Press. ISBN 0198562101.

Benson, R., Garg, R. and Woollatt, D., 1964. "A numerical solution of unsteady flow problems". *International Journal of Mechanical Sciences*, Vol. 6, No. 1, pp. 117–144. ISSN 00207403. doi:10.1016/0020-7403(64)90009-8. URL http://www.sciencedirect.com/science/article/pii/0020740364900098.

Heywood, J., 1989. "Internal combustion engines fundamentals".

Li, X., Wang, W., Zou, X., Zhang, Z., Zhang, W., Zhang, S., Chen, T., Cao, Y. and Chen, Y., 2017. "Simulation and Test Research for Integrated Exhaust Manifold and Hot End Durability". doi:10.4271/2017-01-2432.Copyright.

Liu, J., Schorn, N., Schernus, C. and Peng, L., 1996. "Comparison Studies on the Method of Characteristics and Finite Difference Methods for One-Dimensional Gas Flow through IC Engine Manifold". SAE International Journal of Engines, 412. doi:10.4271/960078. URL http://papers.sae.org/960078/.

Montenegro, G., Onorati, A., Della Torre, A. and Torregrosa, A.J., 2011. "The 3Dcell Approach for the Acoustic Modeling of After-Treatment Devices". *SAE International Journal of Engines*, Vol. 4, No. 2, pp. 2011–24–0215. ISSN 1946-3944. doi:10.4271/2011-24-0215. URL http://papers.sae.org/2011-24-0215/.

Nikita, C., Hardalupas, Y. and Taylor, A., 2015. "Study of Pressure Losses of Unsteady Compressible Flows in Three-Way Junctions". *SAE Technical Paper 2015-24-2399*. doi:10.4271/2015-24-2399.Copyright.

Smith, G.D., 1985. "Numerical solution of partial differential equations : finite difference methods". doi:10.1007/s11214-008-9335-2.

Toro, E.F., 1999. *Riemann Solvers and Numerical Methods for Fluid Dynamics*. Springer Berlin Heidelberg, Berlin, Heidelberg, 2nd edition. ISBN 978-3-662-03917-5. doi:10.1007/978-3-662-03915-1. URL http://link.springer.com/10.1007/978-3-662-03915-1.

Winterbone, D.E. and Pearson, R.J., 2000. *Theory of Engine Manifold Design. Wave Action Methods for IC Engines.*, Vol. C. London : Professional Engineering Pub. ISBN 1 86058 209 5.

7. RESPONSIBILITY NOTICE

The authors are the only responsible for the printed material included in this paper.